ACS APPLIED MATERIALS & INTERFACES

Research Article

www.acsami.org

Samarium and Yttrium Codoped $BaCeO_3$ Proton Conductor with Improved Sinterability and Higher Electrical Conductivity

Zhen Shi,[†] Wenping Sun,*[,†,‡] Zhongtao Wang,[†] Jing Qian,[†] and Wei Liu*[,†,§]

[†]CAS Key Laboratory of Materials for Energy Conversion & Collaborative Innovation Center of Suzhou Nano Science and Technology, University of Science and Technology of China (USTC), Hefei 230026, P.R. China

[‡]School of Materials Science and Engineering, Nanyang Technological University, 50 Nanyang Avenue, Singapore 639798, Singapore

[§]Key Laboratory of Materials Physics, Institute of Solid State Physics, Chinese Academy of Sciences, Hefei 230031, P.R. China

ABSTRACT: Acceptor-doped barium cerate is considered as one of the state-of-the-art high temperature proton conductors (HTPCs), and the proton conductivity of such HTPCs is heavily dependent on the dopant. In this work, a codoping strategy is employed to improve the electrical conductivity and sinterability of $BaCeO_3$-based HTPC. $BaCe_{0.8}Sm_xY_{0.2-x}O_{3-\delta}$ ($0 \le x \le 0.2$) powders are synthesized by a typical citrate−nitrate combustion method. The XRD and Raman spectra reveal all the compounds have an orthorhombic perovskite structure. The effects of Sm and/or Y doping on the sinterability and electrical conductivity under different atmospheres are carefully investigated. The SEM results of the sintered $BaCe_{0.8}Sm_xY_{0.2-x}O_{3-\delta}$ pellets indicate a significant sintering enhancement with increasing Sm concentration. $BaCe_{0.8}Sm_{0.1}Y_{0.1}O_{3-\delta}$ exhibits the highest electrical conductivity in hydrogen among the $BaCe_{0.8}Sm_xY_{0.2-x}O_{3-\delta}$ pellets. Anode-supported $BaCe_{0.8}Sm_{0.1}Y_{0.1}O_{3-\delta}$ electrolyte membranes are also fabricated via a drop-coating process, and the corresponding single cell exhibits desirable power performance and durability at low temperatures. The results demonstrate that $BaCe_{0.8}Sm_{0.1}Y_{0.1}O_{3-\delta}$ is a promising proton conductor with high conductivity and sufficient sinterability for proton-conducting solid oxide fuel cells operating at reduced temperatures.

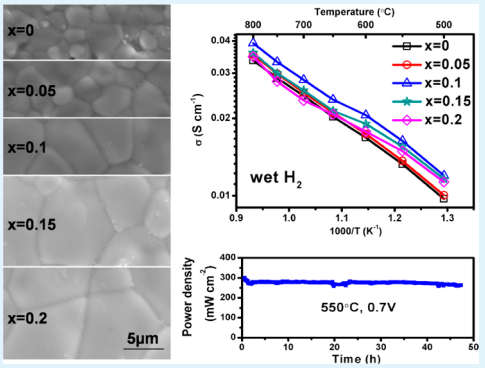

KEYWORDS: *barium cerate, sinterability, electrical conductivity, high temperature proton conductors, solid oxide fuel cells*

1. INTRODUCTION

Acceptor-doped $BaCeO_3$-based high temperature proton conductors (HTPCs) exhibit high proton conductivity at intermediate/low temperatures, and have a great potential in various kinds of applications.[1−3] Compared to the solid oxide fuel cells (SOFCs) with oxygen-ion conducting electrolyte (stabilized zirconia and doped ceria), doped $BaCeO_3$-based proton-conducting SOFCs possess multiple advantages, including lower activation energy for proton transportation and evasion of the internal short circuit in doped ceria electrolytes. In addition to electrode materials, fuel cell performance at reduced temperatures is highly dependent on the ohmic resistance of the cell, which is mainly associated with thickness and conductivity of electrolyte layer. HTPCs also play a key role in other applications, such as hydrogen separation membranes, hydrogen sensors and membrane reactors. It has been widely reported that the hydrogen permeation flux of the conventional metal−ceramics hydrogen separation membranes is usually rate-limited by the proton conductivity of the HTPCs.[4,5] The proton conductivity also affects the sensitivity of hydrogen sensors. Therefore, it is critical to develop HTPCs with sufficiently high proton conductivity to achieve considerable performances for those electrochemical devices.

For $BaCeO_3$-based HTPCs, proton generation and transportation are closely correlated with doped trivalent element, which is well-suggested by experimental and simulation results.[6,7] Additionally, sinterability of $BaCeO_3$ also varies with dopants. Amsif et al. [8] studied $BaCeO_3$ doped with a series of rare-earth elements (La, Nd, Sm, Gd, Yb, Tb, and Y). They demonstrated a dependence of grain size, bulk/grain boundary and total conductivities on the ionic radius of the dopant. $BaCeO_3$ doped with Gd, Y or Sm exhibited relatively high electrical conductivity. Gu et al [9] investigated the dopants' influence on conductivity as well as sintering ability of $BaCe_{0.85}Ln_{0.15}O_{3-\delta}$ (Ln = Gd, Y, Yb) ceramics. Y-doped $BaCeO_{3-\delta}$ shows the highest conductivity while the sintering ability is related to the dopant ionic radius. Besides, the thermodynamically stability is also related to dopants' ionic radius. According to Matskevich et al.'s work on Nd- and Lu-doped $BaCeO_3$,[10] the thermodynamic stability is increasing when ion radius of rare-earth dopant is decreasing. As an attempt to further enhance proton conductivity, codoping strategy[11−13] was implemented in HTPCs, but the effect remains to be further verified. Yang et al. [14] reported $BaZr_{0.1}Ce_{0.7}Y_{0.1}Yb_{0.1}O_{3-\delta}$ (BZCYYb) showed the highest electrical conductivity among the serial compositions of

Received: January 22, 2014
Accepted: March 19, 2014
Published: March 19, 2014

 © 2014 American Chemical Society

$BaZr_{0.1}Ce_{0.7}Y_{0.2-x}Yb_xO_{3-\delta}$ in wet oxygen. However, in our previous work [15] on the Y- and/or Yb-doped $BaCeO_3$-$BaZrO_3$ solid solution, the electrical conductivity of the oxides decreased after substituting Y with Yb in wet hydrogen. In other cases, Su et al. [16] studied $BaCe_{0.8}Nd_xY_{0.2-x}O_{3-\delta}$ and found that the ionic conductivity in air was improved after codoping compared with that of the single-doped ones. Zhao et al. [17] investigated Y and In codoped barium cerate in the form of $BaCe_{0.7}In_xY_{0.3-x}O_{3-\delta}$. They reported that the sintering ability as well as chemical stability increased with In concentration, whereas the electrical conductivity decreased monotonously. According to the definition of Goldschmidt tolerance factor (t), free volume (V_f), and Amsif et al.'s work,[8] Sm increases the lattice distortion (detrimental to ionic conduction) while enlarging the free volume (favors the ionic conduction), when compared to Y. Hence, a proper ratio of Sm:Y is expected to balance the contradictory contribution and achieve high ionic conductivity in samarium and yttrium codoped $BaCeO_3$ serial oxides.

In this work, Sm and Y were employed as dopants to further investigate the codoping effects on the properties of $BaCeO_3$-based HTPCs. The microstructure and electrical conductivity in different atmospheres of the well-sintered $BaCe_{0.8}Sm_xY_{0.2-x}O_{3-\delta}$ (x = 0, 0.05, 0.1, 0.15, 0.2) pellets were studied with the emphasis on a possible relationship among dopant property, sinterability, and proton conductivity.

2. EXPERIMENTAL SECTION

2.1. Powder Synthesis and Pellet Fabrication. $BaCe_{0.8}Sm_xY_{0.2-x}O_{3-\delta}$ (x = 0, 0.05, 0.1, 0.15, 0.2) powders were synthesized via a citric acid−nitrate gel combustion process.[18] First, Y_2O_3 (4N) and/or Sm_2O_3 (3N) are dissolved in nitric acid (AR). Then $Ce(NO_3)_3{\cdot}6H_2O$ (AR) was added followed by $Ba(CH_3COO)_2$ (AR). Afterwards, citric acid (AR) was added at the molar ratio of metal ions:citric acid of 1:1.5. Subsequently, the pH value was adjusted to around 7 with ammonia (AR). The obtained solution was kept stirring at 70 °C until ignition and combustion into ash. The as-prepared powders were calcined at 1000 °C in air for 3 h to form a single perovskite phase. The $BaCe_{0.8}Sm_xY_{0.2-x}O_{3-\delta}$ powders were ground thoroughly with a mortar and pestle before preparing green pellet samples. The $BaCe_{0.8}Sm_xY_{0.2-x}O_{3-\delta}$ pellets were fabricated by a uni-axial pressing method with a pressure of 200 MPa. Afterwards, the pellets were sintered at 1500 °C for 5 h in air to obtain dense pellet samples for conductivity measurement.

2.2. Characterization of $BaCe_{0.8}Sm_xY_{0.2-x}O_{3-\delta}$ powders and pellets. The phase composition of the as-prepared powders and pellets samples were examined by an X-ray diffractometer (XRD; Rigaku TTR-III) with CuKα radiation (λ = 1.54Å). Raman spectra were conducted with a Raman spectrometer (LabRamHR). Scanning electron microscope (SEM; JEOL JSM-6700F) was employed to study the surface and cross-sectional morphology of the sintered pellets. Image-analysis softwares, Nanomeasurer and Image pro plus were utilized to analyze the obtained SEM pictures and count the grain size. The relative density of the sintered pellets was determined via Archimedean method.

Ag paste (PC-Ag-6800, Sino-platinum Metal CO., Ltd) was painted on both sides of each pellet followed by firing at 700 °C for 1 h, obtaining porous electrodes. Ag wire was used as the lead wire. The total resistance of $BaCe_{0.8}Sm_xY_{0.2-x}O_{3-\delta}$ pellets was determined by the electrochemical impedance spectroscopy (EIS) which was performed by an impedance analyzer (CHI604B, Chenhua, Shanghai) in the temperature range of 500−800 °C. The testing atmospheres were dry hydrogen, wet hydrogen (3% H_2O) and dry oxygen in chronological order for each sample. A 5 mA A.C. amplitude signal was applied and the sweeping frequency ranged from 100 kHz to 0.1 Hz. The gas flowing rate was around 50 mL min^{-1}.

2.3. Fuel Cell Fabrication and Testing. The anode supported half cells with tri-layered structure with NiO-$BaCe_{0.8}Sm_{0.1}Y_{0.1}O_{3-\delta}$ (prepared via one-pot combustion process) anode functional layers were fabricated by drop-coating electrolyte suspension on pre-sintered anode substrates and consequently sintered at 1400 °C for 5 h.[19] $Sm_{0.5}Sr_{0.5}Co_{3-\delta}$-$Ce_{0.8}Sm_{0.2}O_{2-\delta}$ composite cathodes were brush-painted on the electrolyte layers and then fired at 950 °C for 2 h.[20] The single cell was tested with a home-made cell testing system with humidified hydrogen (3% H_2O, 30 mL min^{-1}) as the fuel and static air as the oxidant. The I−V curves of the cells were measured with a DC Electronic Load (ITech Electronics model IT8511), and the EIS curves of the cell under open circuit conditions were performed by an impedance analyzer (CHI604B, Chenhua, Shanghai). A 5 mA A.C. amplitude signal was applied and the sweeping frequency ranged from 100 kHz to 0.1 Hz.

3. RESULTS AND DISCUSSION

3.1. Phase Composition. Figure 1 presents the XRD patterns of the $BaCe_{0.8}Sm_xY_{0.2-x}O_{3-\delta}$ powders prepared by the

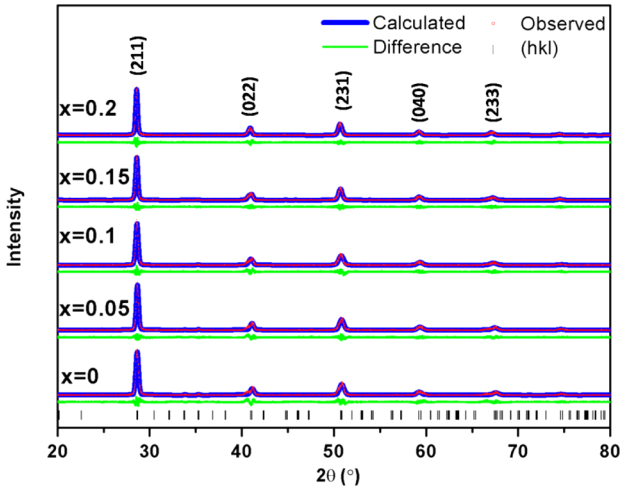

Figure 1. XRD patterns of $BaCe_{0.8}Sm_xY_{0.2-x}O_{3-\delta}$ ($0 \le x \le 0.2$) powders prepared via combustion method and calcined at 1000 °C for 3 h.

combustion method after calcined at 1000 °C for 3 h in air. All the diffraction peaks in the patterns correspond to the orthorhombic perovskite structure,[5] indicating that all the powders possess the same crystal symmetry. A slight peak shift to the lower-angle region can be observed with increasing Sm content, which is attributed to the larger radii of Sm^{3+} (R^{VI} = 0.958 Å) compared to that of Y^{3+} (R^{VI} = 0.90 Å).[21] In Figure 2, all the Raman spectra show strong bands and demonstrate the subtle variation in $BaCe_{0.8}Sm_xY_{0.2-x}O_{3-\delta}$ ceramics. The bands in frequency range of 300−375 cm^{-1} refer to the O-B-O bending in ABO_3.[22−24] According to the Raman spectra of Yb^{3+}-doped (R^{VI} = 0.86 Å), Gd^{3+}-doped (R^{VI} = 0.94 Å), Nd^{3+}-doped (R^{VI} = 1.00 Å), and undoped $BaCeO_3$, it was concluded that increasing ion radii lead to more and more distortion from orthorhombic structure; correspondingly, the number of Raman-active vibration bands decreases, indicating a transition to a more symmetric structure.[23] In our case, all the samples exhibit similar vibration bands, conforming that the phase structure keeps unchanged with varying Sm concentration.

3.2. Sintering. Shown in Figure 3 are SEM images of the cross-sectional (a) and surface (b) morphology of the $BaCe_{0.8}Sm_xY_{0.2-x}O_{3-\delta}$ pellets sintered at 1500 °C for 5 h. The sintering ability as well as the grain size is obviously

dx.doi.org/10.1021/am500467m | ACS Appl. Mater. Interfaces 2014, 6, 5175−5182

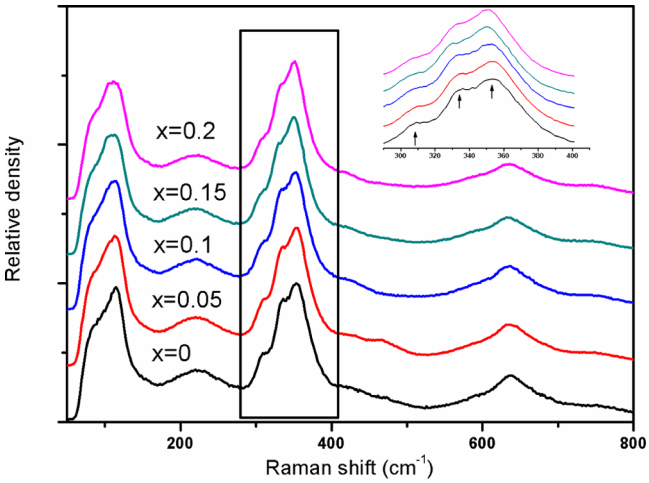

Figure 2. Raman spectra of $BaCe_{0.8}Sm_xY_{0.2-x}O_{3-\delta}$ ($0 \le x \le 0.2$) powders calcined at 1000 °C for 3 h.

improved after Sm incorporation, which agrees with the results reported by Gorbova et al. [6] and Amsif et al. [8] that Sm could promote sinterability of doped barium cerate. The grain size distribution displayed in Figure 4 and average grain size listed in Table 1 further confirms the enhancement. With increasing Sm concentration, the grain size grows larger, resulting in less grain boundary, and this would be beneficial for decreasing grain-boundary resistance.[25] The relative density of the pellets was also performed with a typical Archimedean method (Table 1) and increased correspondingly with Sm concentration.

3.3. Electrical Conductivity. Doped barium cerates exhibit different charge transport behaviors under different atmospheres. The Kroger–Vink notation for the corresponding defect reactions are described below[9]

$$H_2(g) + 2h^{\bullet} + 2O_O^X \rightarrow 2OH_O^{\bullet} \quad (1)$$

$$H_2O + V_O^{\bullet\bullet} + O_O^X \rightarrow 2OH_O^{\bullet} \quad (2)$$

$$H_2O + 2h^{\bullet} + O_O^X \rightarrow 2OH_O^{\bullet} \quad (3)$$

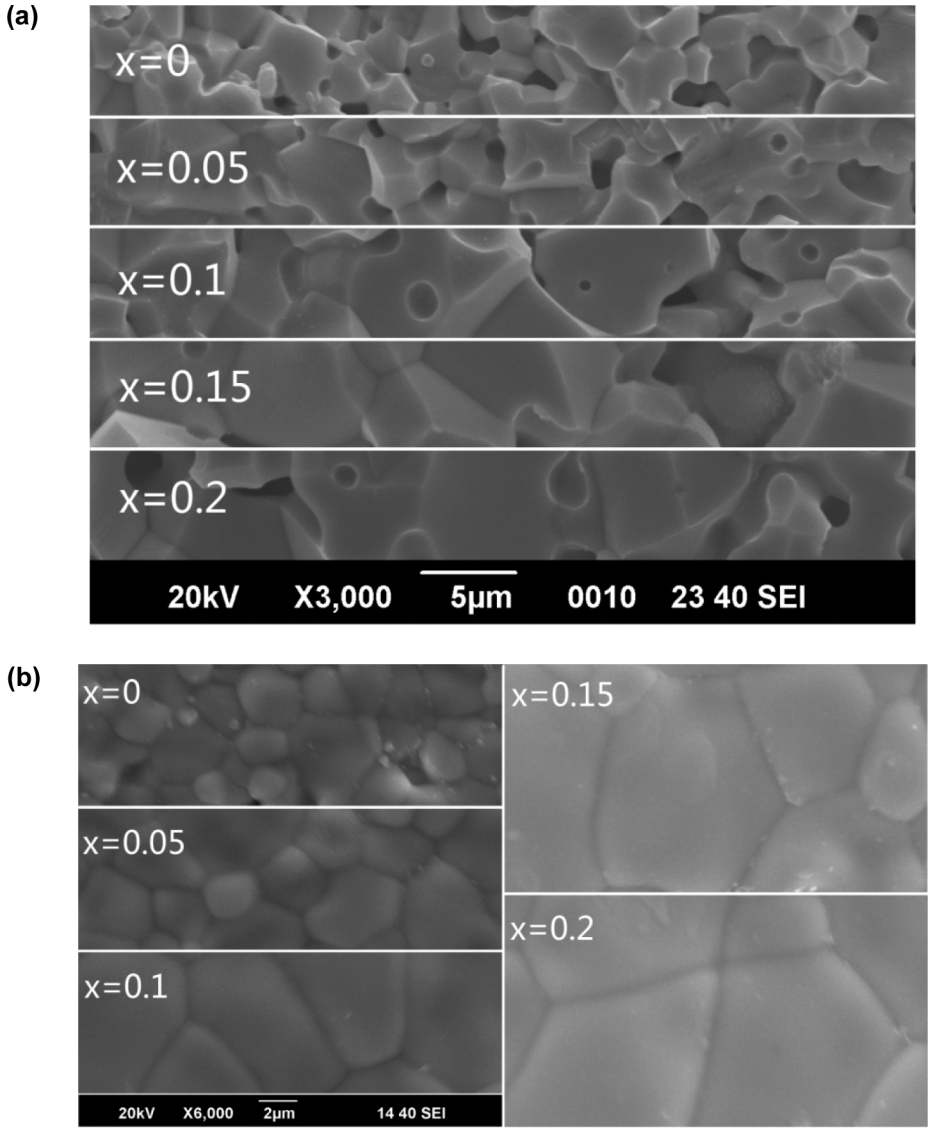

Figure 3. SEM images of the cross-sectional (a) and surface (b) morphology of $BaCe_{0.8}Sm_xY_{0.2-x}O_{3-\delta}$ ($0 \le x \le 0.2$) pellets sintered at 1500 °C for 5 h.

dx.doi.org/10.1021/am500467m | ACS Appl. Mater. Interfaces 2014, 6, 5175–5182

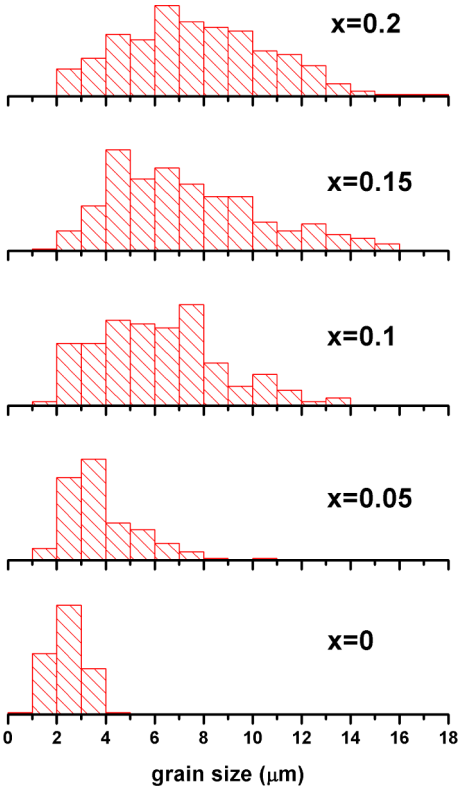

Figure 4. Surface grain size statistics of the sintered $BaCe_{0.8}Sm_xY_{0.2-x}O_{3-\delta}$ ($0 \le x \le 0.2$) pellet samples.

$$\frac{1}{2}O_2(g) + V_O^{\bullet\bullet} \rightarrow O_O^X + 2h^{\bullet} \quad (4)$$

Proton defects in proton conductors may come from H_2 or water vapor, as illustrated in eqs 1−3. Generally, proton conduction dominates the charge transport under H_2O/H_2-containing atmosphere at intermediate/low temperatures (below 700 °C).[26] Doped $BaCeO_3$ exhibit significant electronic conduction contributed by the hole in atmospheres with high oxygen partial pressure, as shown in eq 4. The electronic conductivity would be suppressed after introducing water vapor or in H_2-containing atmosphere,[9] which can be interpreted by eqs 1−3.

Figure 5 shows the total electrical conductivities of $BaCe_{0.8}Sm_{0.1}Y_{0.1}O_{3-\delta}$ under different atmospheres. As restricted by the highest frequency of the impedance analyzer, it is unable to distinguish the bulk resistance and boundary resistance at the testing temperatures, hence only total electrical conductivity was evaluated in this work. Because of the significant contribution from p-type electronic conduction (eq 4),[27] $BaCe_{0.8}Sm_{0.1}Y_{0.1}O_{3-\delta}$ shows much higher electrical conductivity in dry O_2 in the high-temperature region. The conductivity

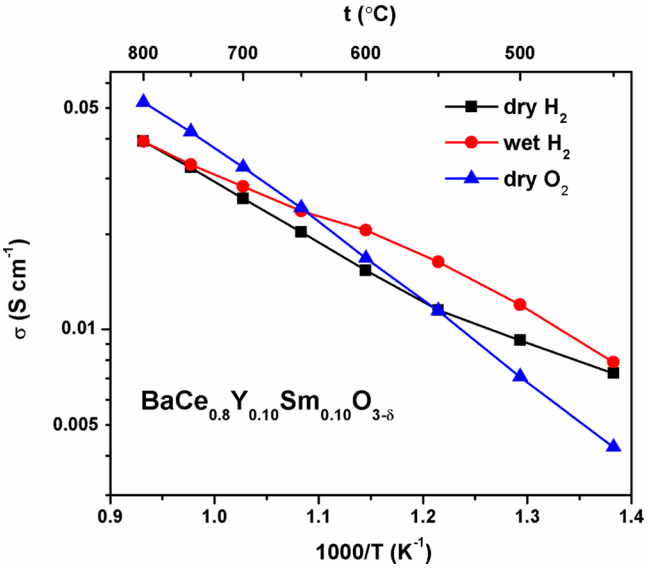

Figure 5. Arrhenius plots of the total electrical conductivity (σ) of $BaCe_{0.8}Sm_{0.1}Y_{0.1}O_{3-\delta}$ pellets under different atmospheres.

superiority in dry O_2 gradually disappears with decreasing temperature due to the higher apparent activation energy for hole hopping (Table 2). The conductivity in wet hydrogen (3% H_2O) is higher than that in dry hydrogen at temperatures lower than 700 °C, in which temperature region proton conduction is predominate and the proton transport number is higher than 0.8.[26] Water vapor contributes a new path for proton incorporation (eq 2) and is beneficial to increase proton concentration and mobility in the oxide,[28] thereby inducing higher proton conductivity in wet hydrogen. Besides, the apparent activation energy for proton conductivity is lowered after introducing water vapor, as presented in Table 2. According to Kreuer et al.'s work,[3] the enthalpy of the hydration reaction tends to become more exothermic with decreasing electronegativity of the cations interacting with the lattice oxygen. Increasing temperature (above 700 °C) would restrain the hydration process and promote water desorption in $BaCeO_3$-based HTPCs.[29] Therefore, water partial pressure

Table 2. Summary of Apparent Activation Energy (E_a, eV) for Electrical Conductivity of $BaCe_{0.8}Sm_xY_{0.2-x}O_{3-\delta}$ under Different Atmospheres

	sample (x)				
	0	0.05	0.1	0.15	0.2
dry H_2	0.41(1)	0.43(7)	0.46(8)	0.47(3)	0.48(4)
wet H_2	0.37(9)	0.37(2)	0.35(1)	0.34(5)	0.33(9)
dry O_2	0.60(6)	0.58(8)	0.56(5)	0.54(1)	0.54(4)

Table 1. Summary of Cell Parameters, Relative Density, and Average Grain Sizes of $BaCe_{0.8}Sm_xY_{0.2-x}O_{3-\delta}$ pellets.

compositions	cell parameters				relative density (%)	D_g (μm)
	a (Å)	b (Å)	c (Å)	V (Å^3)		
$BaCe_{0.8}Y_{0.2}O_{3-\delta}$	8.7320(5)	6.2572(3)	6.2185(4)	339.77(2)	85.5	2.4
$BaCe_{0.8}Sm_{0.05}Y_{0.15}O_{3-\delta}$	8.7457(5)	6.2648(2)	6.2314(4)	341.41(3)	86.4	3.8
$BaCe_{0.8}Sm_{0.1}Y_{0.1}O_{3-\delta}$	8.7560(4)	6.2836(3)	6.2177(4)	342.09(2)	86.9	6.2
$BaCe_{0.8}Sm_{0.15}Y_{0.05}O_{3-\delta}$	8.7649(5)	6.2785(8)	6.2265(6)	342.65(6)	89.4	7.3
$BaCe_{0.8}Sm_{0.2}O_{3-\delta}$	8.7724(5)	6.2904(3)	6.2245(4)	343.48(3)	90.9	7.9

dx.doi.org/10.1021/am500467m | ACS Appl. Mater. Interfaces 2014, 6, 5175−5182

difference has no obvious effect on the proton conductivity at high temperatures. With temperature decreasing, the hydration reaction is more and more thermodynamically favorable. Proton mobility, another factor that influences proton conductivity, decreases with the temperature rapidly and plays an increasingly important role in proton conduction, so the proton conductivity drops under the combined effect of proton mobility and concentration. As a consequence, the total proton conductivity become similar again at further reduced temperatures (below 500 °C) as shown in Figure 5. Azad et al. [30] also reported an analogous electrical conductivity relationship under different water vapor-containing atmospheres in Ba-$(Ce,Zr)_{1-x}Sc_xO_{3-\delta}$ perovskites.

Figure 6 reveals the Arrhenius plots of the electrical conductivity of $BaCe_{0.8}Sm_xY_{0.2-x}O_{3-\delta}$ in dry and wet hydrogen (3% H_2O). In dry hydrogen (Figure 6a), the conductivity first increases with the Sm concentration build-up, and tops at x=0.1, with a total conductivity of 3.92×10^{-2} S cm^{-1} for $BaCe_{0.8}Sm_{0.1}Y_{0.1}O_{3-\delta}$ at 800 °C. When Sm content continues to increase, the total conductivity starts to drop and reaches the minimum at $x = 0.2$ (3.48×10^{-2} S cm^{-1} at 800 °C). In wet H_2 (3% H_2O) (Figure 6b), the tendency is similar to that in dry H_2. And the total conductivity varies with x in the following sequence: 0.1 > 0.15 > 0.05 > 0 > 0.2. According to the equations discussed above, the main charge carrier is proton in the two atmospheres. As is widely reported,[8,31] proton trapping and mobility is closely associated with the dopants incorporated into the Ce sites of $BaCeO_3$. Gu et al. [9] investigated the influence of dopants on conductivity as well as sintering ability of a series of $BaCe_{0.85}Ln_{0.15}O_{3-\delta}$ (Ln = Gd, Y, Yb) ceramics. Y-doped $BaCeO_{3-\delta}$ shows the highest conductivity while the sintering ability is also related to dopant ionic radius. Amsif et al.[8,32] studied $BaCe_{0.9}Ln_{0.1}O_{3-\delta}$ containing rare-earth dopants with different ionic radii and found that the conductivity reaches a maximum for Gd-doped samples rather than Y. Besides, their results also inferred that Y and Sm exhibit enhanced impacts on the electrical properties of barium cerates. Table 3 lists a comparative study on total electrical conductivity in the present work with the data from literatures at 600 °C, in order to demonstrate the difference induced by codoping Y and Sm in $BaCeO_{3-\delta}$. In this work, the total proton conductivity of $BaCe_{0.8}Sm_xY_{0.2-x}O_{3-\delta}$ is determined by the proton mobility and grain size. Increasing Sm concentration is detrimental to proton mobility, but this enhances sintering and generates larger grain sizes (Figure 3), which would decrease grain boundary density and thereby grain-boundary resistance.[25]

However, Sm-doping has a totally positive effect on the electrical conductivity of $BaCe_{0.8}Sm_xY_{0.2-x}O_{3-\delta}$ in dry oxygen (Figure 6c). In dry oxygen, holes and oxygen ions become the main charge carriers. And the apparent activation energy rises from around 0.4 eV to about 0.6 eV (Table 2). In this case, the improved conductivity is mainly induced by the improved grain size and decreased grain-boundary density.

3.4. Single Cell Performance. In order to further evaluate the electrochemical performance as an electrolyte material, single cells with thin $BaCe_{0.8}Sm_{0.1}Y_{0.1}O_{3-\delta}$ electrolyte membranes and $Sm_{0.5}Sr_{0.5}Co_{3-\delta}$-$Ce_{0.8}Sm_{0.2}O_{2-\delta}$ (SSC-SDC) composite cathodes were prepared and tested. The SEM image of the cross-sectional morphology of the as-prepared single cell is displayed in Figure 7. The electrolyte membrane is around 16 μm in thickness, fully dense, free from crack, and bonds firmly to the electrode membranes. The fuel cell power performance is shown in Figure 8a. The peak power density (PPD) achieved

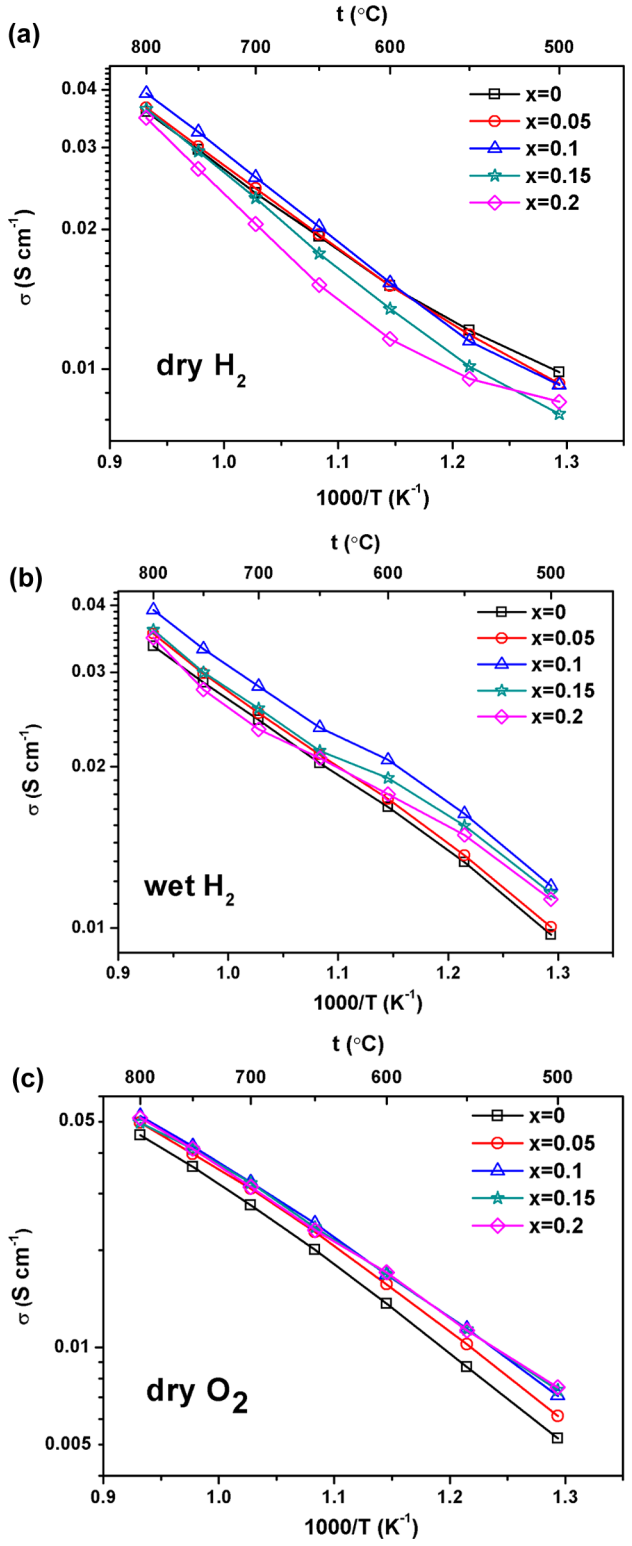

Figure 6. Arrhenius plots of $BaCe_{0.8}Sm_xY_{0.2-x}O_{3-\delta}$ with different Sm content under different atmospheres: (a) dry hydrogen, (b) wet hydrogen (3% H_2O), and (c) dry oxygen.

0.60, 0.51, and 0.36 W cm^{-2} at 650, 600 and 550 °C, respectively, and the fuel cell still delivered power densities of 0.49, 0.41 and 0.28 W cm^{-2} at a working voltage of 0.7 V. The cell performance was significantly improved compared to some other previously reported doped $BaCeO_3$-based fuel cells, as presented in Table 4. Bi et al. [33] prepared a 16 μm thick

dx.doi.org/10.1021/am500467m | ACS Appl. Mater. Interfaces 2014, 6, 5175−5182

Table 3. Comparative Study on Total Electrical Conductivity in the Present Work with the Data from the Literatures at 600 °C

materials	measured conditions	σ ($\times 10^{-2}$ S cm^{-1}, 600 °C)	ref
$BaCe_{0.8}Sm_{0.1}Y_{0.1}O_{3-\delta}$	3% H_2O-H_2	2.37	this work
$BaCe_{0.8}Sm_{0.2}O_{3-\delta}$	3% H_2O-H_2	2.07	this work
$BaCe_{0.8}Y_{0.2}O_{3-\delta}$	3% H_2O-H_2	2.04	this work
$BaCe_{0.85}Y_{0.15}O_{3-\delta}$	4% H_2O-H_2	2.11	9
$BaCe_{0.85}Gd_{0.15}O_{3-\delta}$	4% H_2O-H_2	2.01	9
$BaCe_{0.9}Y_{0.1}O_{3-\delta}$	wet 5% H_2-Ar	1.35	8
$BaCe_{0.9}Gd_{0.1}O_{3-\delta}$	wet 5% H_2 – Ar	2.00	8
$BaCe_{0.9}Nd_{0.1}O_{3-\delta}$	wet 5% H_2 – Ar	0.49	37
$BaCe_{0.8}Sm_{0.2}O_{3-\delta}$	wet 5% H_2 – Ar	1.70	38

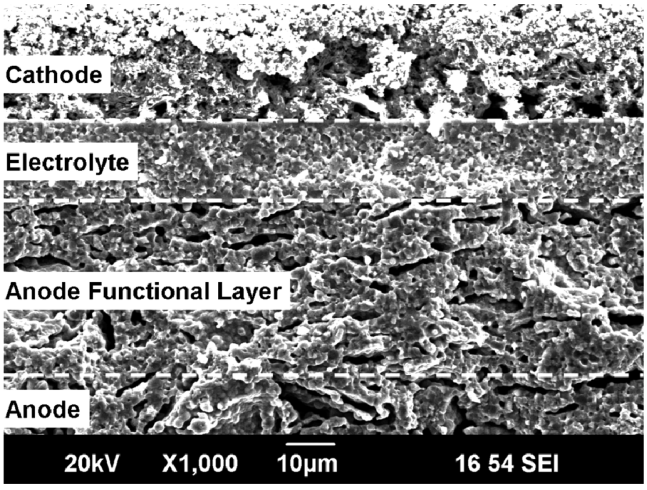

Figure 7. SEM image of cross-sectional morphology of the as-prepared $BaCe_{0.8}Sm_{0.1}Y_{0.1}O_{3-\delta}$-based single cell.

$BaCe_{0.8}Sm_{0.2}O_{3-\delta}$ electrolyte layer via screen printing, and the corresponding peak power density of the single cell was 0.24 and 0.13 W cm^{-2} at 650 and 600 °C, respectively. Tao et al. [34] reported a fuel cell with a 20 μm thick Ga-doped $BaCeO_3$ electrolyte membranes, only outputting peak power density of 0.15 W cm^{-2} at 650 °C. The inferior performances mainly induced by the high area-specific ohmic (R_{ohm}) and polarization (R_p) resistance of the cells. The electrochemical impedance spectra (EIS) (Figure 8b) measured under open circuit conditions reveal that the $BaCe_{0.8}Sm_{0.1}Y_{0.1}O_{3-\delta}$-based fuel cell shows much lower R_{ohm} and R_p values, as shown in Table 4, which should be responsible for the power performance. The R_{ohm} value is 0.35, 0.37 and 0.44 Ω cm^2, whereas R_p is only 0.05, 0.20, and 0.49 Ω cm^2 at 650, 600, and 550 °C, respectively. The lower R_{ohm} and R_p values can be attributed to the thin and dense electrolyte membranes with high proton conductivity, highly electro-active cathode material and fine electrode microstructure. Besides, the conductivity of the $BaCe_{0.8}Sm_{0.1}Y_{0.1}O_{3-\delta}$ electrolyte membranes under fuel cell conditions was also estimated according to the film thickness and R_{ohm} values, achieving about 4.2×10^{-3}, 4.0×10^{-3}, and 3.4×10^{-3} S cm^{-1} at 650, 600, and 550 °C, respectively. It should be mentioned that the film conductivity is lower than the pellet sample, suggesting that R_{ohm} value of the cell can be further reduced by optimizing the cell fabrication process. Thus, it can

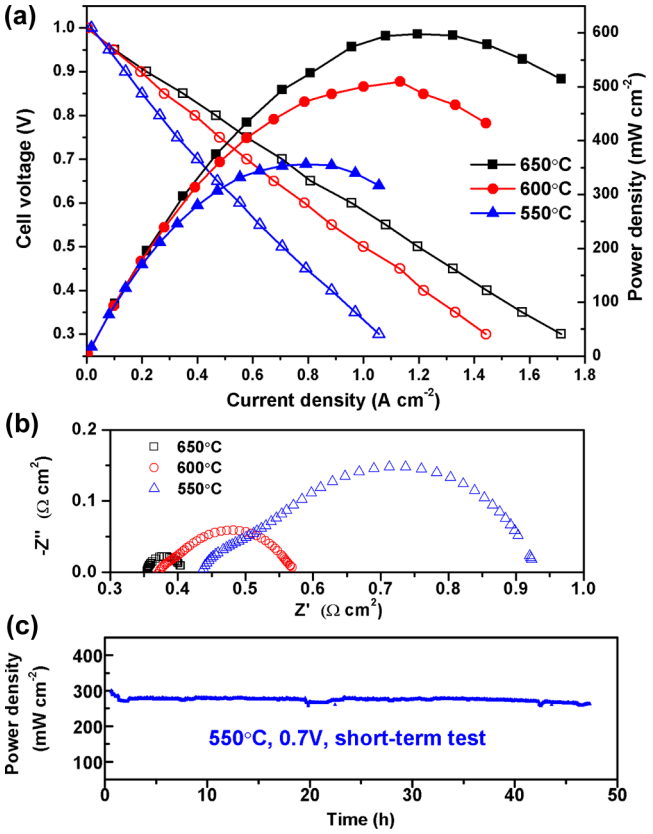

Figure 8. (a) $I-V$ and power density curves, (b) electrochemical impedance spectra under open circuit conditions, and (c) short-term stability testing of the $BaCe_{0.8}Sm_{0.1}Y_{0.1}O_{3-\delta}$-based single cell with wet hydrogen (3% H_2O) as the fuel and static air as the oxidant.

be anticipated that there is still much room to enhance cell performance.

Suffering from the well-known thermodynamic instability, especially under water vapor and CO_2-containing atmospheres, dope $BaCeO_3$ is facing serious challenges for working as a durable electrolyte material for SOFCs. The short-term performance stability of the $BaCe_{0.8}Sm_{0.1}Y_{0.1}O_{3-\delta}$-based fuel cell was evaluated at a low temperature of 550 °C with a constant output voltage of 0.7 V. One can see from Figure 8c that the power density nearly keeps constant without significant degradation after operating for 47 h. The good durability of the cell performance can be ascribed to the reduced operating temperature as well as the well-sintered dense electrolyte film which provided less active sites for corrosion. Park et al. [35] reported a stable electrochemical performance of $BaCe_{0.8}Sm_{0.2}O_{3-\delta}$-based cells, outputting 0.36 W cm^{-2} at 700 °C for 24 h without degradation even after one thermal cycle. Peng et al. [36] also carried out durability test with $BaCe_{0.8}Sm_{0.2}O_{3-\delta}$ electrolyte at 650 °C for 1000 min, and they found that the cell performance showed no obvious decline at a working voltage of 0.7 V and current density of around 0.12 A cm^{-2}. To further examine the chemical stability of the electrolyte, the anode supported dense $BaCe_{0.8}Sm_{0.1}Y_{0.1}O_{3-\delta}$ electrolyte film was treated at 600 °C for 12 h under flowing wet air (~3% H_2O), as the electrolyte film is exposed in similar atmosphere under SOFC operating conditions. The XRD patterns (Figure 9) indicate that the dense electrolyte membranes survive the test and no obvious reaction occurs. The results imply that $BaCeO_3$-based proton

dx.doi.org/10.1021/am500467m | ACS Appl. Mater. Interfaces 2014, 6, 5175−5182

Table 4. Summary of the Electrolyte Film Thickness (μm), Cathode Material, R_{ohm} and R_P (Ω cm^2), and Peak Power Density (W cm^{-2}) of the Cells with Doped $BaCeO_3$-Based Proton Conductors Reported in Literature

electrolyte	thickness	cathode	R_{ohm}	R_p	PPD	ref
$BaCe_{0.8}Sm_{0.2}O_{3-\delta}$	10	LSF-BCS	0.25	0.61	0.54 (650 °C)	39
$BaCe_{0.8}Ga_{0.2}O_{3-\delta}$	20	LSCF-BZCY	1.22	2.09	0.10 (600 °C)	34
$BaCe_{0.8}Sm_{0.2}O_{3-\delta}$	50	BSCF-BCS	1.13	2.17	0.13 (600 °C)	36
$BaCe_{0.8}Y_{0.2}O_{3-\delta}$	10	Pd			0.37 (600 °C)	40
$BaCe_{0.8}Sm_{0.2}O_{3-\delta}$	16	LSF- BCS	0.70	1.05	0.12 (600 °C)	33
$BaCe_{0.8}Sm_{0.1}Y_{0.1}O_{3-\delta}$	16	SSC- SDC	0.37	0.20	0.51 (600 °C)	this work

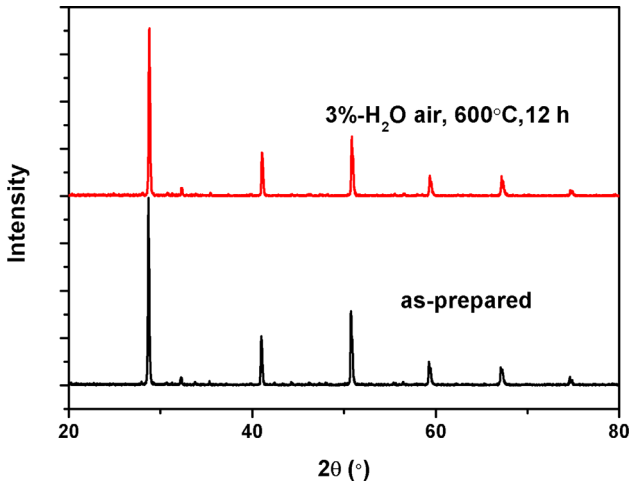

Figure 9. XRD patterns of the dense $BaCe_{0.8}Sm_{0.1}Y_{0.1}O_{3-\delta}$ electrolyte film before and after exposure in flowing wet air (~3% H_2O) at 600 °C for 12 h.

conductors are durable electrolyte materials for SOFCs operating at reduced temperatures. Overall, it is crucial to improve the conductivity of doped $BaCeO_3$, explore highly active electrode materials and optimize the cell microstructures for further lowering the operating temperature of $BaCeO_3$-based fuel cells.

4. CONCLUSIONS

In this work, the dopant effect on the electrical conductivity and sinterability of $BaCe_{0.8}Sm_xY_{0.2-x}O_{3-\delta}$ (x = 0, 0.05, 0.1, 0.15, 0.2) proton conductors was carefully studied. Sm could effectively promote the sinterability of $BaCe_{0.8}Sm_xY_{0.2-x}O_{3-\delta}$, whereas is detrimental to proton transportation. The conductivity variation of $BaCe_{0.8}Sm_xY_{0.2-x}O_{3-\delta}$ polycrystalline ceramics is determined by proton mobility and grain boundary density. Sinterability and bulk conductivity reaches a compromise in $BaCe_{0.8}Sm_{0.1}Y_{0.1}O_{3-\delta}$, which exhibits the highest total proton conductivity with sufficient sinterability among the series. Moreover, $BaCe_{0.8}Sm_{0.1}Y_{0.1}O_{3-\delta}$-based single cells outputted excellent power density and good short-term stability. Doped barium cerate is a promising durable proton conducting electrolyte material for low-temperature solid oxide fuel cells.

AUTHOR INFORMATION

Corresponding Authors

*Tel: +86 0551 63606929; Fax: +86 0551 63602586. E-mail: swp@mail.ustc.edu.cn.

*E-mail: wliu@ustc.edu.cn.

Notes

The authors declare no competing financial interest.

ACKNOWLEDGMENTS

This work was supported by Ministry of Science and Technology of China (Grant 2012CB215403). The project was also supported by research fund of Key Laboratory for Advanced Technology in Environmental Protection of Jiangsu Province.

REFERENCES

(1) Iwahara, H. Hydrogen Pumps Using Proton-Conducting Ceramics and Their Applications. *Solid State Ionics* **1999**, *125* (1-4), 271−278.

(2) Iwahara, H. Proton Conducting Ceramics and Their Applications. *Solid State Ionics* **1996**, *86-8*, 9−15.

(3) Kreuer, K. D. Proton-Conducting Oxides. *Annu. Rev. Mater. Res.* **2003**, *33* (1), 333−359.

(4) Zhu, Z.; Sun, W.; Yan, L.; Liu, W.; Liu, W. Synthesis and Hydrogen Permeation of Ni−$Ba(Zr_{0.1}Ce_{0.7}Y_{0.2})O_{3-\delta}$ Metal−Ceramic Asymmetric Membranes. *Int. J. Hydrogen Energy* **2011**, *36* (10), 6337−6342.

(5) Medvedev, D.; Murashkina, A.; Pikalova, E.; Demin, A.; Podias, A.; Tsiakaras, P. $BaCeO_3$: Materials Development, Properties and Application. *Prog. Mater. Sci.* **2014**, *60*, 72−129.

(6) Gorbova, E.; Maragou, V.; Medvedev, D.; Demin, A.; Tsiakaras, P. Investigation of the Protonic Conduction in Sm Doped $BaCeO_3$. *J. Power Sources* **2008**, *181* (2), 207−213.

(7) Kreuer, K. D. Aspects of the Formation and Mobility of Protonic Charge Carriers and the Stability of Perovskite-Type Oxides. *Solid State Ionics* **1999**, *125* (1-4), 285−302.

(8) Amsif, M.; Marrero-Lopez, D.; Ruiz-Morales, J. C.; Savvin, S. N.; Gabas, M.; Nunez, P. Influence of Rare-Earth Doping on the Microstructure and Conductivity of $BaCe_{0.9}Ln_{0.1}O_{3-\delta}$ Proton Conductors. *J. Power Sources* **2011**, *196* (7), 3461−3469.

(9) Gu, Y.-J.; Liu, Z.-G.; Ouyang, J.-H.; Yan, F.-Y.; Zhou, Y. Structure and Electrical Conductivity of $BaCe_{0.85}Ln_{0.15}O_{3-\delta}$ (Ln = Gd, Y, Yb) Ceramics. *Electrochim. Acta* **2013**, *105*, 547−553.

(10) Matskevich, N. I.; Wolf, T.; Matskevich, M. Y.; Chupakhina, T. I. Preparation, Stability and Thermodynamic Properties of Nd- and Lu-Doped $BaCeO_3$ Proton-Conducting Ceramics. *Eur. J. Inorg. Chem.* **2009**, *2009* (11), 1477−1482.

(11) Sun, W. P.; Liu, M. F.; Liu, W. Chemically Stable Yttrium and Tin Co-Doped Barium Zirconate Electrolyte for Next Generation High Performance Proton-Conducting Solid Oxide Fuel Cells. *Adv. Energy Mater.* **2013**, *3* (8), 1041−1050.

(12) Xie, K.; Yan, R.; Xu, X.; Liu, X.; Meng, G. A Stable and Thin $BaCe_{0.7}Nb_{0.1}Gd_{0.2}O_{3-\delta}$ Membrane Prepared by Simple All-Solid-State Process for SOFC. *J. Power Sources* **2009**, *187* (2), 403−406.

(13) Fabbri, E.; D'Epifanio, A.; Di Bartolomeo, E.; Licoccia, S.; Traversa, E. Tailoring the Chemical Stability of $Ba(Ce_{0.8-x}Zr_x)Y_{0.2}O_{3-\delta}$ Protonic Conductors for Intermediate Temperature Solid Oxide Fuel Cells (IT-SOFCs). *Solid State Ionics* **2008**, *179* (15-16), 558−564.

(14) Yang, L.; Wang, S.; Blinn, K.; Liu, M.; Liu, Z.; Cheng, Z.; Liu, M. Enhanced Sulfur and Coking Tolerance of a Mixed Ion Conductor for SOFCs: $BaZr_{0.1}Ce_{0.7}Y_{0.2-x}Yb_xO_{3-\delta}$. *Science* **2009**, *326* (5949), 126−9.

(15) Shi, Z.; Sun, W.; Liu, W. Synthesis and Characterization of $BaZr_{0.3}Ce_{0.5}Y_{0.2-x}Yb_xO_{3-\delta}$ Proton Conductor for Solid Oxide Fuel Cells. *J. Power Sources* **2014**, *245*, 953−957.
(16) Su, X.; Yan, Q.; Ma, X.; Zhang, W.; Ge, C. Effect of Co-dopant Addition on the Properties of Yttrium and Neodymium Doped Barium Cerate Electrolyte. *Solid State Ionics* **2006**, *177* (11-12), 1041−1045.
(17) Zhao, F.; Liu, Q.; Wang, S. W.; Brinkman, K.; Chen, F. L. Synthesis and Characterization of $BaIn_{0.3-x}Y_xCe_{0.7}O_{3-\delta}$ (x = 0, 0.1, 0.2, 0.3) Proton Conductors. *Int. J. Hydrogen Energy* **2010**, *35* (9), 4258−4263.
(18) Zhu, Z.; Yan, L.; Sun, W.; Liu, H.; Liu, T.; Liu, W. A Cobalt-Free Composite Cathode Prepared by a Superior Method for Intermediate Temperature Solid Oxide Fuel Cells. *J. Power Sources* **2012**, *217*, 431−436.
(19) Liu, M.; Dong, D.; Peng, R.; Gao, J.; Diwu, J.; Liu, X.; Meng, G. YSZ-Based SOFC with Modified Electrode/Electrolyte Interfaces for Operating at Temperature Lower than 650°C. *J. Power Sources* **2008**, *180* (1), 215−220.
(20) Sun, W. P.; Yan, L. T.; Lin, B.; Zhang, S. Q.; Liu, W. High Performance Proton-Conducting Solid Oxide Fuel Cells with a Stable $Sm_{0.5}Sr_{0.5}Co_{3-\delta}$−$Ce_{0.8}Sm_{0.2}O_{2-\delta}$ Composite Cathode. *J. Power Sources* **2010**, *195* (10), 3155−3158.
(21) Shannon, R. D. Revised Effective Ionic-Radii and Systematic Studies of Interatomic Distances in Halides and Chalcogenides. *Acta Crystallogr., Sect. A* **1976**, *32*, 751−767.
(22) Sun, W. P.; Jiang, Y. Z.; Wang, Y. F.; Fang, S. M.; Zhu, Z. W.; Liu, W.; Novel, A Electronic Current-Blocked Stable Mixed Ionic Conductor for Solid Oxide Fuel Cells. *J. Power Sources* **2011**, *196* (1), 62−68.
(23) Scherban, T.; Villeneuve, R.; Abello, L.; Lucazeau, G. Raman-Scattering Study of Acceptor-Doped $BaCeO_3$. *Solid State Ionics* **1993**, *61* (1-3), 93−98.
(24) Liu, M.; Sun, W.; Li, X.; Feng, S.; Ding, D.; Chen, D.; Liu, M.; Park, H. C. High-Performance Ni−$BaZr_{0.1}Ce_{0.7}Y_{0.1}Yb_{0.1}O_{3-\delta}$ (BZCYYb) Membranes for Hydrogen Separation. *Int. J. Hydrogen Energy* **2013**, *38* (34), 14743−14749.
(25) Haile, S. M.; Staneff, G.; Ryu, K. H. Non-Stoichiometry, Grain Boundary Transport and Chemical Stability of Proton Conducting Perovskites. *J. Mater. Sci.* **2001**, *36* (5), 1149−1160.
(26) Iwahara, H.; Yajima, T.; Ushida, H. Effect of Ionic-Radii of Dopants on Mixed Ionic-Conduction (H^++O^{2-}) in $BaCeO_3$-Based Electrolytes. *Solid State Ionics* **1994**, *70*, 267−271.
(27) Di Bartolomeo, E.; D'Epifanio, A.; Pugnalini, C.; Zunic, M.; D'Ottavi, C.; Licoccia, S. Phase Stability and Electrochemical Analysis of Nb Doped $BaCe_{0.9}Y_{0.1}O_{3-x}$ Electrolyte for IT-SOFCs. *ECS Trans.* **2010**, *28* (11), 259−265.
(28) Coors, W. G.; Readey, D. W. Proton Conductivity Measurements in Yttrium Barium Cerate by Impedance Spectroscopy. *J. Am. Ceram. Soc.* **2002**, *85* (11), 2637−2640.
(29) Saiful Islam, M. Ionic Transport in ABO_3 Perovskite Oxides: a Computer Modelling Tour. *J. Mater. Chem.* **2000**, *10* (4), 1027−1038.
(30) Azad, A.; Irvine, J. Synthesis, Chemical Stability and Proton Conductivity of the Perovksites $Ba(Ce,Zr)_{1-x}Sc_xO_{3-\delta}$. *Solid State Ionics* **2007**, *178* (7-10), 635−640.
(31) Lv, J.; Wang, L.; Lei, D.; Guo, H.; Kumar, R. V. Sintering, Chemical Stability and Electrical Conductivity of the Perovskite Proton Conductors $BaCe_{0.45}Zr_{0.45}M_{0.1}O_{3-\delta}$ (M = In, Y, Gd, Sm). *J. Alloys Compd.* **2009**, *467* (1-2), 376−382.
(32) Amsif, M.; Marrero-Lopez, D.; Ruiz-Morales, J. C.; Savvin, S. N.; Nunez, P. Effect of Sintering Aids on the Conductivity of $BaCe_{0.9}Ln_{0.1}O_{3-\delta}$. *J. Power Sources* **2011**, *196* (22), 9154−9163.
(33) Bi, L.; Zhang, S.; Lin, B.; Fang, S.; Xia, C.; Liu, W. Screen-Printed $BaCe_{0.8}Sm_{0.2}O_{3-\delta}$ Thin Membrane Solid Oxide Fuel Cells with Surface Modification by Spray Coating. *J. Alloys Compd.* **2009**, *473* (1-2), 48−52.
(34) Tao, Z.; Zhu, Z.; Wang, H.; Liu, W. A Stable $BaCeO_3$-Based Proton Conductor for Intermediate-Temperature Solid Oxide Fuel Cells. *J. Power Sources* **2010**, *195* (11), 3481−3484.
(35) Park, I.; Kim, J.; Lee, H.; Park, J.; Shin, D. $BaCeO_3$−$BaCe_{0.8}Sm_{0.2}O_{3-\delta}$ bi-Layer Electrolyte-Based Protonic Ceramic Fuel Cell. *Solid State Ionics* **2013**, *252*, 152−156.
(36) Ranran, P.; Yan, W.; Lizhai, Y.; Zongqiang, M. Electrochemical Properties of Intermediate-Temperature SOFCs Based on Proton Conducting Sm-Doped $BaCeO_3$ Electrolyte Thin Film. *Solid State Ionics* **2006**, *177* (3-4), 389−393.
(37) Zhang, C.; Zhao, H. Electrical Conduction Behavior of Sr Substituted Proton Conductor $Ba_{1-x}Sr_xCe_{0.9}Nd_{0.1}O_{3-\delta}$. *Solid State Ionics* **2010**, *181* (33), 1478−1485.
(38) Zhang, C.; Zhao, H. Influence of In Content on the Electrical Conduction Behavior of Sm-and In-Co-Doped Proton Conductor $BaCe_{0.80-x}Sm_{0.20}In_xO_{3-\delta}$. *Solid State Ionics* **2012**, *206*, 17−21.
(39) Bi, L.; Zhang, S.; Fang, S.; Zhang, L.; Xie, K.; Xia, C.; Liu, W. Preparation of an Extremely Dense $BaCe_{0.8}Sm_{0.2}O_{3-\delta}$ Thin Membrane Based on an In Situ Reaction. *Electrochem. Commun.* **2008**, *10* (7), 1005−1007.
(40) Balachandran, U. B.; Lee, T. H.; Dorris, S. E. SOFC Based on Proton Conductors. *ECS Trans.* **2007**, *7* (1), 987−992.